LC-DET-2006-005

ILC Beam Energy Measurement based on Synchrotron Radiation from a Magnetic Spectrometer

K. Hiller[1], R. Makarov[2], H.J. Schreiber[1], E. Syresin[3], B. Zalikhanov[3]

[1]DESY, Platanenallee 6, D-15738 Zeuthen, Germany

[2]Moscow State University, 119899 Moscow, Russia

[3]Dzhelepov Laboratory of Nuclear Problems, JINR, 141980 Dubna, Moscow Region, Russia

Abstract

We propose to measure, on a bunch-to-bunch basis, the beam energy at the International Linear e^+e^- Collider by monitoring synchrotron radiation (SR) light emitted in the magnets of an energy spectrometer based on beam position monitors. Measuring the width of the horizontal SR fan permits to determine the relative beam energy with a precision better than 10^{-4}. There are two different measuring schemes possible. The first one is based on edge measurements of the direct SR fan, while the second option includes mirrors to deflect soft SR light to detectors located sufficiently off the beamline. Three possibilities for high-spatial resolution detectors are considered: a standard silicon strip detector, a novel-type Si detector with exceptional position resolution and a gas amplification detector. The main issue of the first scheme is the high radiation dose expected in the direct SR fan. If mirrors are used this dose is strongly reduced and allows application of any of the three detectors proposed.

1 Introduction

The International Linear Collider (ILC) physics program requires to measure particle masses of e.g. the Higgs boson and the top quark with uncertainties of about 50 MeV. Since the beam energy uncertainty has a major impact on the accuracy of the mass measurements, a precision of 100 parts per million (ppm) for incident beam energy measurements is needed. In order to achieve this goal, a beam position monitor (BPM)-based magnetic spectrometer was proposed to perform single-bunch measurements with a precision of $\Delta E_b/E_b \simeq 5 \cdot 10^{-5}$ [1]. The determination of E_b with such an error relies on precise information of beam positions from BPM's with 100 nm resolution upstream and downstream of the spectrometer magnet and a relative B-field integral tolerance of $2 \cdot 10^{-5}$.

A complementary method of beam energy measurement based on synchrotron radiation (SR) emitted in the dipole magnets of the energy spectrometer was proposed in [2]. Measuring the SR fan at far distances downstream of the spectrometer provides a precise independent beam energy monitoring when both horizontal edge positions of the fan are known with micrometer precision [3].

An energy spectrometer based on synchrotron radiation was used at SLAC for precision measurements of the SLC beam energy [4, 5]. Horizontal SR stripes created in two horizontal bending magnets were incident on fine wire arrays. The position of the two stripes separated by an analyzing magnet was determined by measuring the charge ejected from the wires by the incident radiation, so that the deflection angle of the beam in the magnet was directly accessible. The beam energy was measured with a resolution better than 250 ppm at 45 GeV with very good long-term stability.

In this paper we propose to monitor the ILC beam energy with an uncertainty better than 10^{-4} using either the direct synchrotron radiation photons (scheme 1) or photons deflected by mirrors in the energy range up to 20 keV (scheme 2). Fast and radiation-resistant detectors with high spatial resolution are required for both schemes. Often used silicon strip detectors are suited for precise position measurements. Novel-type Si detectors for registration of photons with large spatial resolution or gas amplification solid state detectors proposed in this note are also options for our demands.

The paper is organized as follows. Sect. 2 describes basic properties of synchrotron radiation light expected from the spectrometer described in ref.[1]. Possible experimental schemes for beam energy determination are explored in Sect.3, while results from GEANT simulations are presented in Sect.4. In Sect.5 basic methods for measurements of γ-quanta in an energy regime relevant for our study and their physical limitations are discussed. This is followed in Sect.6 by discussions on possible synchrotron radiation detectors with excellent spatial resolution which might be suitable for both schemes. Sect.7 contains the conclusions.

2 Synchrotron Radiation from the Energy Spectrometer

The spectrometer proposed in [1], used as an example in this note, consists of three bending magnets: two ancillary magnets and one spectrometer magnet as seen in Fig.1. At the nominal beam energy of 250 GeV, the spectrometer magnetic rigidity corresponds to 0.84 Tm for a magnet length of 3 m. The distance between the ancillary and spectrometer magnets is 10 m and the length of the ancillary magnet 1.5 m. The electrons/positrons which pass through the magnets emit synchrotron radiation. Its monitoring at some distance to the spectrometer permits determination of E_b via the energy-versus-bending angle dependence. We assume that the SR detector is placed 80 m downstream from the center of the spectrometer magnet. The size of the SR horizontal fan respectively the position of its edges are defined by the energy of the beam particles, the field strength of the magnets and the geometry of the set-up.

Basic features of the SR produced within the spectrometer magnet by means of GEANT3 [6] are summarized in Figs.2 and 3. The multiplicity of the photons emitted by a beam particle is shown in Fig.2. The avarage number of photons $< N_\gamma >$ is about 5 with a tail up to 14, resulting to a total number of γ's produced in the spectrometer magnet of 10^{11} for $2 \cdot 10^{10}$ particles per bunch. This number agrees well with the analytical estimation of $< N_\gamma >= 5/(2\sqrt{3})\alpha e B \cdot l/2mc = 5.3$, where $B \cdot l$ is the magnetic rigidity, m and e the electron mass respectively charge, c the velocity of light and $\alpha = 1/137$. Fig.3 shows the energy distribution of the

photons. The energy spectrum peaks at values below 1 MeV and has a long exponential tail above the critical photon energy up to about 100 MeV. The average photon energy $< E_\gamma >$ amounts to 3.8 MeV, which is in good agreement with the estimated value of $< E_\gamma >= (8\sqrt{3}/45) \cdot E_{cr} = 3.6$ MeV, with the critical energy $E_{cr} \simeq 0.65 \cdot E_b^2[GeV] \cdot B[T] = 11.6$ MeV for the 250 GeV nominal beam energy. The simulated photon energy spectrum shown in Fig.3 coincides with the estimated SR spectrum $dN_\gamma/dE_\gamma \approx 0.4 \cdot N_\gamma \cdot (E_\gamma/E_{cr})^{1/3}/E_\gamma$ at low photon energies, $E_\gamma \ll E_{cr}$.

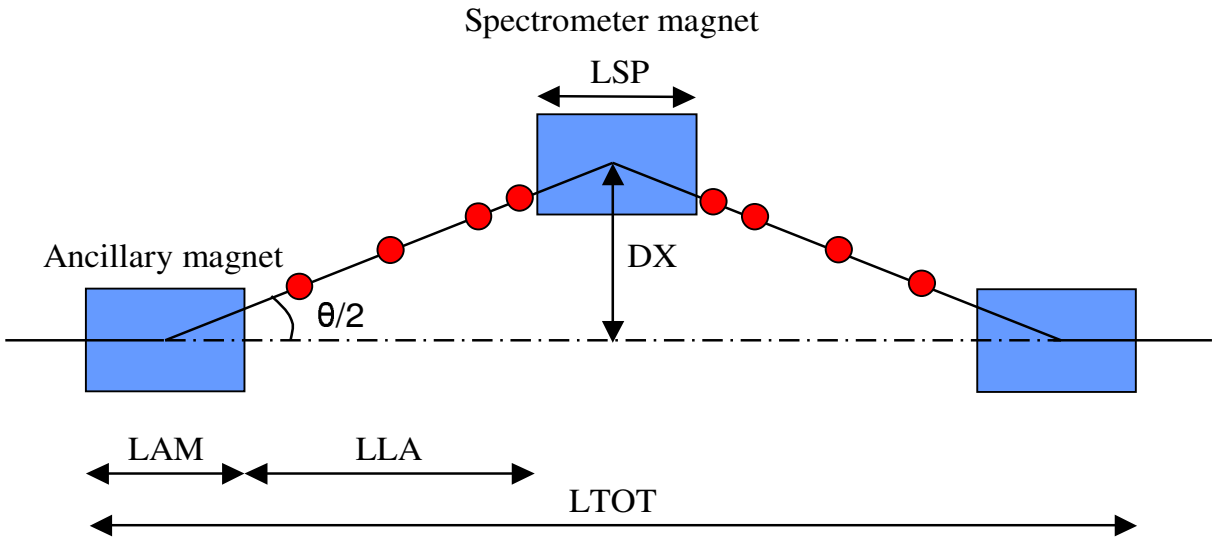

Figure 1: Schematic layout of the magnetic spectrometer as proposed in [1]for ILC beam energy measurements. The circles indicate beam position monitors (BPMs).

Throughout our study we define the z-axis as the direction of the beam, the x-axis in the horizontal or bending plane as indicated in Fig.1 and the y-axis such that a right-handed coordinate system is obtained.

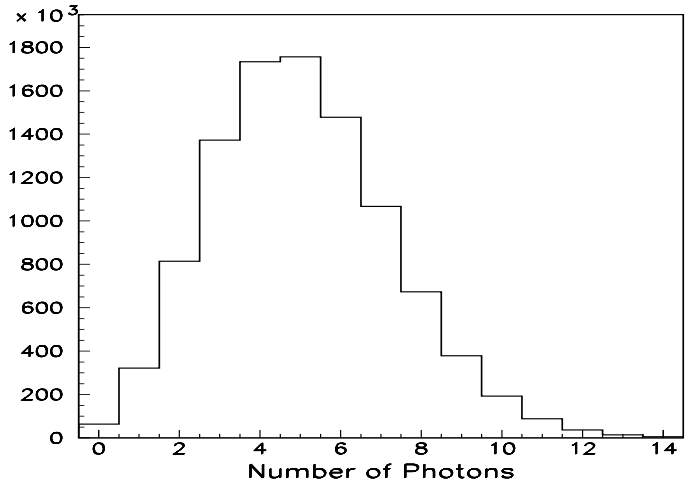

Figure 2: Multiplicity of photons radiated by an electron within the spectrometer magnet.

The electron deflection angle $\theta = eB \cdot l/E_b c$ is defined by the magnetic rigidity $B \cdot l$ and the beam energy E_b. For a rigidity of 0.84 Tm respectively a B-field strength of 0.28 T of the analyzing magnet, the deflecting angle results to $\theta = 1$ mrad at $E_b = 250$ GeV. The x-position of the endpoints of the SR fan are inversely proportional to E_b, $x_{edge} \propto E_b^{-1}$. This endpoint variation with beam energy constitutes the basic concept of monitoring E_b. As an example, Fig.4 shows the complete horizontal SR fan at a distance of 80 m from the center of the spectrometer magnet. An asymmetry of the fan with respect to $x = 0$ and a two-step behaviour

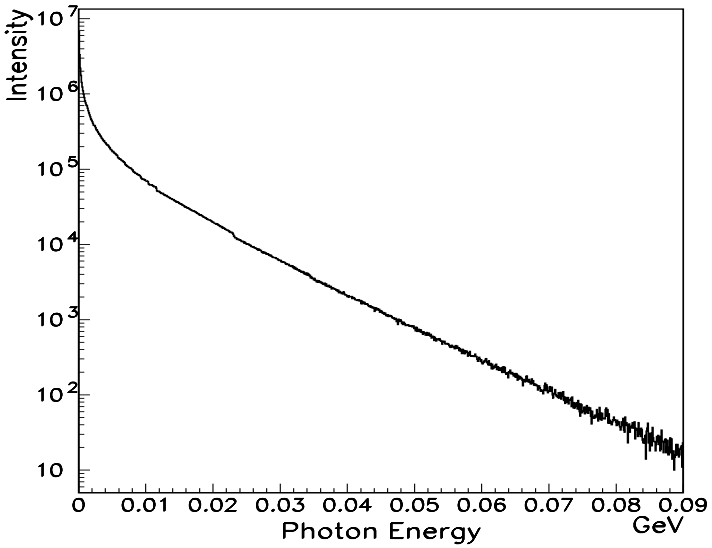

Figure 3: Energy of photons radiated within the spectrometer magnet.

of the intensity are related to the superposition of the SR fans of the three magnets. The intensity step is due to to the different distances of the ancillary magnets to the photon detector. The second ancillary magnet generates a somewhat larger photon density at negative x-values since it is closer to the detector. The position of the right edge $x_{right} = L_1\theta/2 \simeq +46$ mm is determined by the distance of the first ancillary magnet to the detector plane of $L_1 = 92.25$ m and the deflection angle θ, while the left edge location $x_{left} = L_2\theta/2 \simeq$ -34 mm is given by θ and the distance of 80 m to the detector. Hence, the total horizontal width of the SR fan results to ~80 mm at $z = 80$ m downstream of the center of the analyzing magnet.

For stable magnetic fields the vertical size of the SR fan is mainly determined by the photon energy. Photons with energies close to the critical energy generate a vertical divergence of $\theta_{vert} \simeq (E_b/mc^2)^{-1} \simeq 2$ μrad, while photons with energies $E_\gamma \lesssim 20$ keV a larger spread of $\theta_{vert} \simeq 0.5 \cdot (\lambda/R)^{1/3} \simeq 12$ μrad, with λ the photon wavelength and R the curvature radius of the electron trajectories in the spectrometer magnet. The vertical spot size for such photons corresponds to $\Delta y \simeq L_1 \cdot \theta_{vert} \simeq 1.1$ mm, with a rather weak beam energy endpoint position variation of $E_b^{-1/3}$.

The variation of the horizontal SR edge positions with the beam energy and the magnetic field strength permits a determination of the beam energy with an uncertainty of $\Delta E_b/E_b \simeq [(\Delta x/x)^2 + (\Delta Bl/Bl)^2 + (\Delta L/L)^2]^{1/2}$. For an edge position resolution of $\Delta x \simeq 2\mu$m, a precision of $\Delta E_b/E_b \simeq 5 \cdot 10^{-5}$ can be achieved if a relative error for the magnetic rigidity of $\Delta B \cdot l/B \cdot l \simeq 2 \cdot 10^{-5}$ and a tolerance for the distance to the detector of $\Delta L/L \simeq 5 \cdot 10^{-6}$ are assumed. Since the uncertainties anticipated for the B-field and the distance L seem to be feasible, the most critical quantity $\Delta x/x$ requires high-spatial resolution synchrotron radiation detectors.

Ideally, the SR spectrum has sharp cut-offs at both sides as seen in Fig.4. Precise measurement of the SR edges is however hampered by several effects which result to some smearing of the edges.

The SR light is higly collimated in the forward direction with a characteristic energy dependent opening angle θ_{sr}. The angular spread in the horizontal plane is similar to that in the vertical plane: for soft photons with energies of 10 keV the opening angle is almost 12 μrad while it is only 2 μrad for hard photons of a few MeV. This angular variation leads 80 m further downstream at the position of the photon detectors to a broadening of the edges of $\sim 1000\mu$m and 160μm for soft and hard photons, respectively.

Other contributions are related to the finite transverse beam size and the energy spread of the electrons within a bunch. The horizontal beam size which varies typically between 10 and 100 μm within the beam

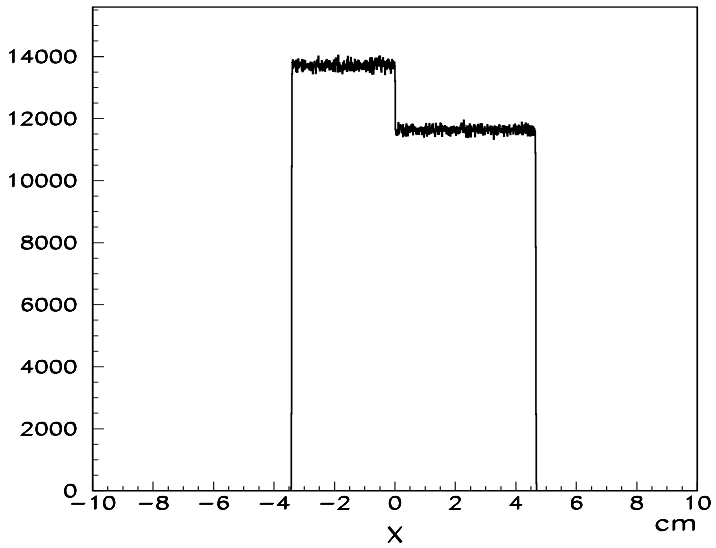

Figure 4: Horizontal coordinate x of the SR fan (arbitrary units) at L = 80 m, E_b = 250 GeV and $B \cdot l$ = 0.84 Tm.

delivery system is directly passed to an edge dilution increment. An electron beam energy spread of $1.5 \cdot 10^{-3}$ leads to a broadening of the edges of about 40 μm due to different particle trajectories in the bending magnets.

Fringe fields of the spectrometer magnets broaden the SR edges due to an increased field strength outside the pole gaps. If a 1 % fraction of the stronly varying fringe field is assumed the corresponding broadening is 100 μm.

Also optical surface errors of the mirrors (scheme 2) contribute to an additional edge smearing. Depending on the manufactoring process the reflection error is in the range of 0.1 to 1.0 arcsec. For a 30 m distance between the mirrors and the detector the reflection error contributes between 15 and 150 μm to the edge broadening.

Uncorrelated ground-motion of the magnets in horizontal direction may generate steps in the synchrotron radiation spectrum near the endpoints. Since frequencies and amplitudes of ground-motions are however strongly site dependent, it is difficult to account for them even qualitatively at the present stage of the project. This effect is largely removed if, as proposed in [1], a compact energy spectrometer with a common concrete girder for the magnets is envisaged. Vertical set-up component vibrations are expected to be harmless due to their orthogonality to the bending plane and the vertical detector layer orientation.

Taking the quadratic sum of the smearing effects considered one expects a SR edge broadening in the order of 1000 μm or less. Including some safety margin, the sensitive horizontal area of the detector has to be at least 5 mm on each side of the fan to enable appropriate registration of SR γ-quanta. This range has furthermore to accomodate possible jitters of the beam position and angle as well as to provide a sufficiently large acceptance region for endpoint determination procedures.

3 Experimental Set-up

In both schemes we propose to measure only that fraction of the synchrotron radiation which is close to the edges of the fan. In scheme 1, the photons are supposed to be accepted by the few millimeter sensitive area of the detectors located 80 m further downstream as shown in Fig.5a. The photons are assumed to move towards the detectors without interactions with the wall of the vacuum chamber. At the end of the

set-up, Roman Pots are installed which contain the detectors. If the beampipe diameter does not increase continuously to sufficiently large values photon collisions will occur and a large fractions of photons will be absorbed. The remaining photons do not allow precise endpoint determinations as can be seen in Fig.6. The Roman Pots are separated by a thin window from the beamline and can be kept under more moderate vacuum, or even no vacuum at all. In this way, the detector front-end electronics and readout cables allow somewhat easier access. However, performance degradation of the detectors within the intense synchrotron radiation enviroment has to be studied. For some discussion and possible solutions we refer to Sect.6.1.

The second scheme of E_b monitoring relies on endpoint position measurements of the SR fan using mirrors. Since the proposed mirrors reflect only photons with $E_\gamma \lesssim 20keV$ their amount expected in the detector is at most $N_\gamma \simeq N_0(\Delta E_\gamma/E_{cr})^{1/3} \simeq 2.5 \cdot 10^{10}$, with $N_0 \simeq 2 \cdot 10^{11}$ the total number of γ-quanta produced in the magnets per bunch, E_{cr} the critical photon energy and ΔE_γ the selected photon energy range of less than 20 keV. To employ the low-energy photons for endpoint measurements, two highly reflective mirrors into the SR fan are proposed to be implemented to deflect soft γ-quanta towards the detectors outside of the fan. The mirrors should be placed at an optimized position somewhere between the spectrometer and the Roman Pots, with a gap between them to avoid interactions with beam particles, as sketched in Fig.5b. Mirrors of 50 cm length are assumed to cover sufficiently large edge regions of the fan. The

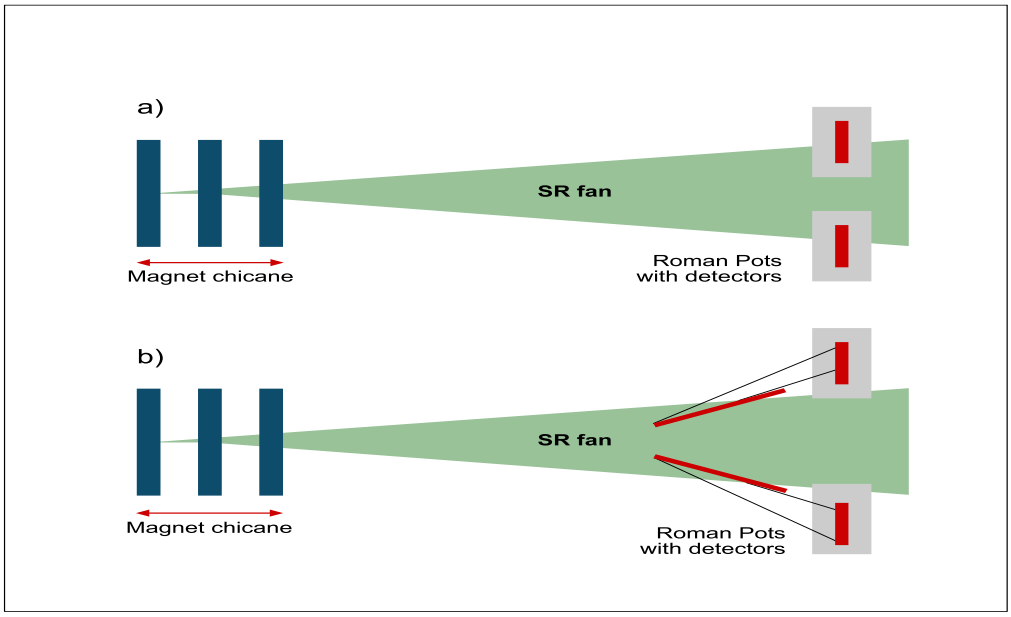

Figure 5: The two schemes for measuring the ILC beam energy by synchrotron radiation emitted within the magnets of the energy spectrometer.

mirrors should have large atomic number Z to select γ-quanta with energies below some cut-off value with high reflectivity. Rhodium (Rh) is supposed to be a suitable material. As long as the reflection angle is smaller than $\phi_{max} \simeq 0.08/E_\gamma[\text{keV}] = 4$ mrad, large reflectivity is ensured. This can be seen in Fig.7, where the reflectivity is shown as a function of the photon energy [7]. If the mirrors are inclined by e.g. 3 mrad with respect to the z-axis, photons with $E_\gamma < 20$ keV are deflected with ~95 % efficiency, while those with larger energies will either pass the reflector or be absorbed. Such a scheme deflects soft photons sufficiently far from the beamline outside the SR fan and avoids serious radiation damages of the detectors. Energy deposited in the mirrors and resulting heating problems should however be estimated as soon as a technical design for the mirror system exists. A streched Rh foil, for example, might lead to an acceptable heat load without a cooling system.

It is also worth to note that the energy resolution for scheme 2 is additionally degraded by $4L_{M-D}\Delta\phi/(\theta \cdot L)$,

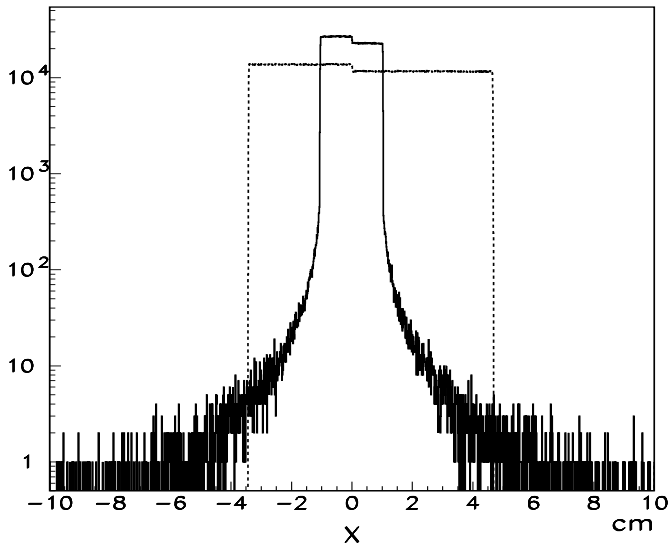

Figure 6: SR spectra (arbitrary units) with/without interactions in 2 mm stainless steel of the 1 cm radius vacuum chamber.

where L_{M-D} is the distance between the mirror and the detector, L the distance to the detectors of 80 m, θ the bending angle of the analyzing magnet and $\Delta\phi$ the light reflection error of the mirrors. If $\Delta\phi$ cannot be kept sufficiently small, L_{M-D} has to be decreased as much as possible in order not to compromise the beam energy resolution too much.

4 GEANT Simulations

The synchrotron light produced in the spectrometer magnets was simulated by means of GEANT3 [6]. The simulation includes effects due to the intrinsic beam energy spread, the beam sizes, the fringe fields, and selects, if required, a sufficient fraction of γ-quanta with $E_\gamma < 20$ keV by means of two mirrors. GEANT tracks the photons through the set-up to the detectors where they are recorded for further studies.

For illustrative purposes, synchrotron radiation fans generated for three beam energies, 250.0 and 250.0 $\pm$0.250 GeV, detected 80 m downstream of the spectrometer center are shown in Fig.8. Photons were deflected by two mirrors with an inclination of 3 mrad positioned 50 m downstream from the chicane. The edge positions of the spectra were obtained by a four-parameter fit. The function to be fitted results from a step-function folded by a Gaussian as proposed in e.g. [8], with the position, the width, the amplitude of the edges and the slope as free parameters. The results of the fit are also shown in Fig.8. Very good χ^2/NDF were obtained and the errors of the edge position were found to be few tenths of a micrometer. When the beam energy increases by 250 MeV the right edge (at negative x-values) shrinks by $\Delta x_R = 32$ μm and the left edge (at positive x-values) by $\Delta x_L = 48$ μm towards smaller $|x|$-values, i.e. the total width of the fan decreases by 80 μm. For a 25 MeV beam energy increase, which corresponds to $\Delta E_b/E_b = 1 \cdot 10^{-4}$, the corresponding edge values shrink by 4 respectively 6 μm so that the total width of the fan is 10 μm smaller. Fig.9 shows the variation of the SR width as a function of the beam energy shifted by $\pm$250 and $\pm$25 MeV. The errors of the width values are in between 0.4 and 0.8 μm and are not visible in Fig.9. The line represents a linear function through the two energy points at $\pm$250 MeV, and its prediction at $\pm$25 MeV agrees with the simulation results within 1.2 μm. From the $\Delta E_b = \pm 250$ MeV values, a sensitivity of 80 μm/250 MeV can be derived, which implies a relative beam energy uncertainty of $\sim 3 \cdot 10^{-5}$ for 2 μm endpoint position resolution.

More pronounced variations of the SR spectra with E_b can be noted if their differences are plotted. Fig.10

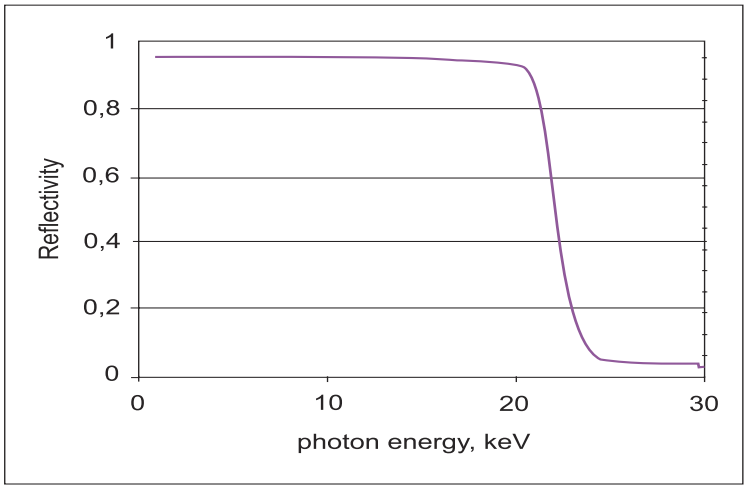

Figure 7: Dependence of Rh mirror reflectivity on photon energy.

shows an example of such difference plots for beam energy shifts of ± 25 MeV with respect to the nominal beam energy. Clear dip respectively bump structures are visible which demonstrate the large sensitivity to the edge variation with E_b. Significant structures are expected to be visible even for less beam energy variations, e.g. for 8 MeV, which corresponds to $\Delta E_b/E_b \simeq 3 \cdot 10^{-5}$.

5 Synchrotron Radiation Detection

Table 1 summarizes photon conversion processes relevant for our study. Passing through matter, photons with energies less than ~100 keV may be absorbed by an atomic electron with subsequent ejection of the electron from the atom, the so-called photoelectric effect. If the photon energy exceeds 100 keV or if its energy is large with respect to the electron binding energy Compton scattering occurs. Both of these interactions give rise to electrons capable of ionizing atoms within the detector medium, which makes it possible to study the spatial dependence of the incoming photons.

	Photoelectric Effect	Compton Scattering	Pair Production
SR interaction	Bound electrons	Free electrons	Atomic nucleus
Energy variation	E^{-3}	E^{-1}	E
Energy range	<100 keV	100 keV-10 MeV	>1.02 MeV(≈10 MeV)
Charge variation	Z^3	None	Z

Table 1. Processes of X-ray conversion into low-energy photons, electrons or positrons.

Since each interaction of photons with atoms leads either to a complete disappearance of the quantum or to an appreciable change of its direction, the intensity of the incident beam exponentially decreases with material thickness d, $\overline{N} = \overline{N_0}e^{-\mu d}$, with $\overline{N_0}$ the initial beam intensity, d the absorber thickness [g/cm^2] and μ the absorption or attanuation coefficient [cm^2/g]. Since the photoelectric cross section varies with the third power of the atomic number Z, higher Z materials are most favored for photoelectric absorption. The ejected electrons undergo large energy loss in high-Z materials and hence a small path length, so that detection with excellent spatial resolution is possible. Thus either a solid state with large Z or a heavy gas with high pressure is suitable for precise localization of incident low-energy γ-rays in matter.

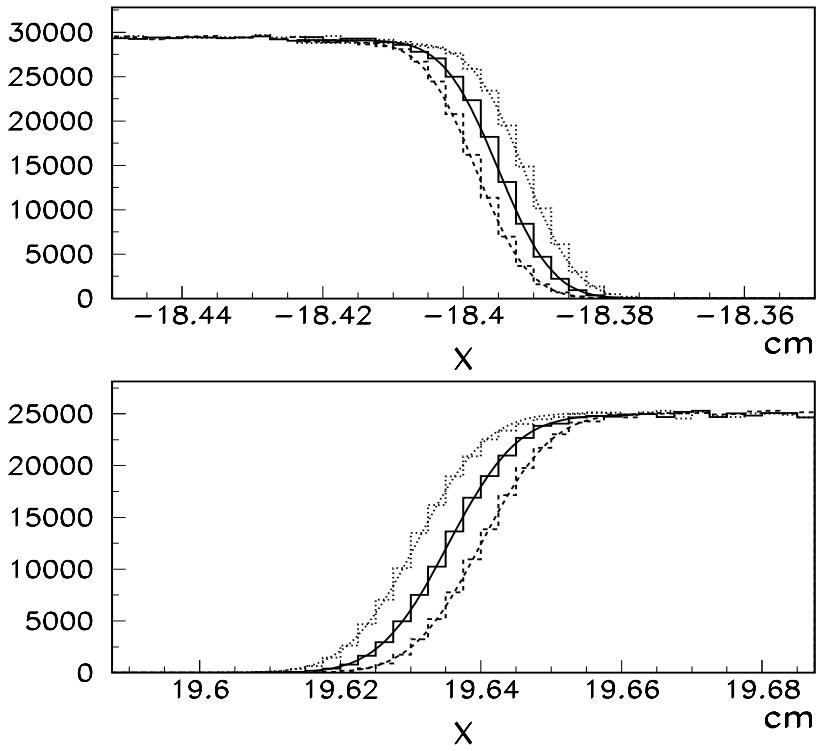

Figure 8: Mirror deflected synchrotron radiation spectra (arbitrary units) for $E_b = 250$ (solid histogram) and 250.0 ± 0.250 GeV versus x coordinate close to the right and left fan edges. The curves are the results of the fit, see the text. Note the edges of the fan for divergent γ-rays are interchanged by the mirrors.

The Compton effect caused by scattering of γ-quanta on free electrons[1] leads to a spatial distribution of the scattered electrons considerable spoiled and therefore to a worse position detection. It is therefore advantageous to select photons with small energies, e.g. of less than 20 keV, where only photoelectric absorption occurs.

The main limitation of the photoelectric process on the spatial resolution is due to the probabilistic nature of the angular distribution and the path length of the photoelectrons along their way through matter. At small energies, the electrons escape mainly perpendicular to the incident γ direction, whereas for large energies they are mainly produced forward. Mean path length values of photoelectrons in gases and solid states as given e.g. in refs.[9, 10] reveal that in aluminim for example, the path length is 2.6 μm for 20 keV electrons. Since the mean path length depends only slightly on the material, the use of a denser medium reduces the length by only 15-20 %. Or, for photons with an energy of 10 keV which are totally absorbed within 1.3 mm Al the path length of the ejected electrons is only 0.4 μm. These numbers indicate the potential to build high-spatial resolution detectors for low-energy photons.

6 High-spatial Resolution Photon Detectors

In our approach of measuring E_b on a bunch-to-buch basis it is intended to monitor variations of the endpoints of the horizontal SR fan with respect to a certain reference point within the detector system. This requires radiation hard high-spatial resolution detectors with large enough acceptance regions on each side of the fan. Due to possible beam position, angle and energy jitters, energy spread within a bunch,

[1] In matter, the electrons are bound. If the radiation energy is however high with respect to the binding energy, this latter energy can be ignored and the electron can be considered as essentially free.

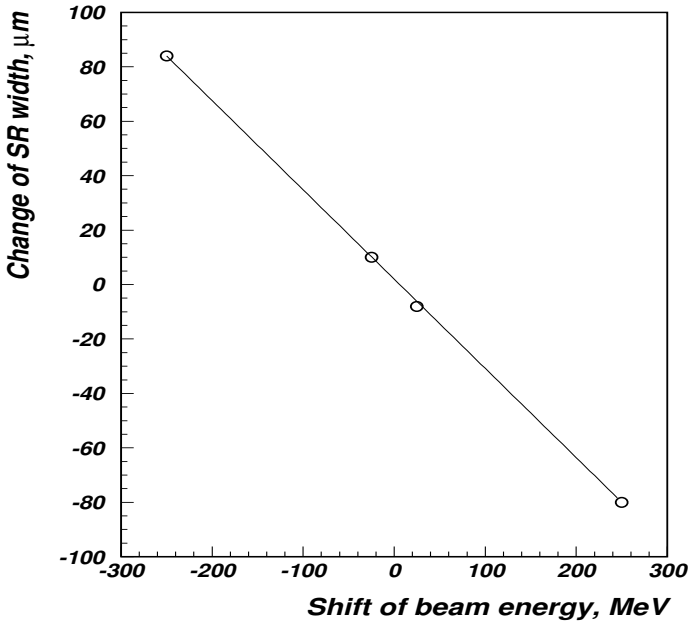

Figure 9: SR width variation as a function of the relative beam energy shift. The straight line is the result of a fit, see the text.

vibration of the magnets and Roman Pots, SR angular divergence etc., the sensitive areas of the detector should be at least 5 mm on each side. The final choice of the acceptance region will depend on the results of detailed simulations of all processes causing smearing and shifts of the endpoints as soon as a final BPM-based spectrometer design for the ILC exists.

6.1 Silicon Strip Detectors

Out of all abundant detector options, silicon strip detectors are suitable for our task. Applied frequently in particle physics experiments, such detectors have demostrated their ability to achieve few micrometer spatial resolution for particle tracking [11]. An ionizing particle traversing the Si detector volume produces electron-hole pairs due to Coulomb interaction, Bremsstrahlung and scattering with the electrons along its path. Per electron-hole pair a mean energy deposit of 3.6 eV is needed. The electric field in the depleted volume causes a drift of the electrons and holes to the positive respectively negative electrode. The induced current is amplified and integrated resulting in a voltage signal proportional to the total charge.

The spatial resolution of silicon detectors is obtained by a segmentation of the anode (p^+) into so-called microstripes. The microstripes might only be ten micrometer apart and this pitch determines the detector resolution. Using only binary-readout single strip signals the spatial resolution is given by $pitch/\sqrt{12}$ what can be improved substantially by employing the charge division method. The spatial resolution of large scale silicon strip detectors with a pitch of e.g. 25 μm can be better than 5 μm.

Silicon detectors were also applied for photon detection in experiments with X-rays or synchrotron radiation [12]. Electrons delivered by photon collisions will produce electron-hole pairs in a thin 300 μm silicon detector with however a small and very energy dependent interaction rate. The typical detection efficiency of individual photons above 100 keV is on the percent level.

For edge measurements of the SR fan as proposed in this study the total number of photons is about 10 times the number of electrons per bunch. Taking into account all relevant physical processes the interaction rate per photon is about 0.5 %. Due to the large number of photons per bunch and a 25 μm readout pitch, for example, sufficient electron-hole pairs are produced allowing for a precise determination of the edge

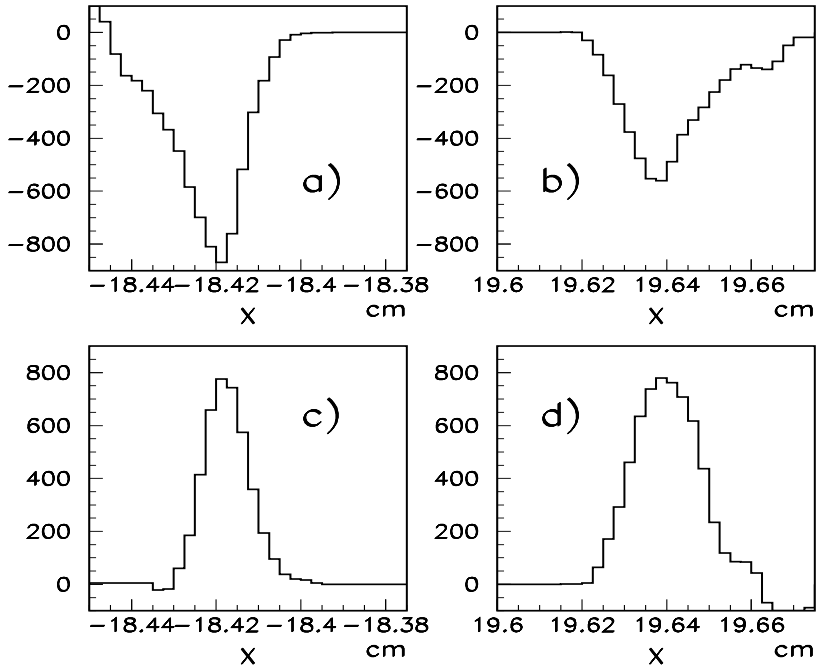

Figure 10: Differences of mirror deflected synchrotron radiation spectra for $E_b = 250$ and 250.0 ± 0.0250 GeV versus x coordinate close to the right (a) and c)) and left (b) and d)) fan edges.

positions. The small size and full depletion of the detector offer a fast response time. Charge collection can be performed in less than 10 ns. If all channels will be readout large scale integration techniques allow to include associated electronics. A Si detector of 5 mm sensitive area and 25 μm pitch would have about 200 readout channels. Such a device with its small volume of electronics required is very advantageous.

The amount of radiation in the direct synchrotron radiation fan expected per year is however so large that radiation damage of the bulk silicon is a critical issue. Since the detector would probably not withstand a dose of more than 1 Mrad [13], dose reduction of orders of magnitude must be achieved. Otherwise, long-term measurements within the direct synchrotron radiation fan with a silicon strip detector is not possible. Radiation hard detectors with high-spatial resolution and sufficient capability for low-energy photon detection are required. Examples are discussed in Sects. 6.2 and 6.3. Or one needs to maintain suitable arrangements for radical reduction of the photon flow. For example, installation of mirrors in the SR fan to deflect only a small fraction of the light to the detectors while the main photon stream passes the sensors, ensures the radiation reduction needed.

In this respect it is worth to mention that detector developers intend to launch an R&D program for e.g. the European XFEL project [14] towards position sensitive detectors applied in a regime very similar to that at the ILC[2]. The demands for the detectors are to a great extent very similar to our needs.

6.2 A Novel-type High Resolution Silicon Detector

In this section a new type of detector with excellent spatial resolution is considered which relies on semiconducting material. Transition processes in semiconductors are described by the equation $d\rho_{fr}/dt + \gamma_1 \rho_{fr}/\varepsilon_a = 0$ [15], where ρ_{fr} is the free volume charge, $\epsilon_a = \varepsilon\varepsilon_0$ the absolute permittivity and γ_1 the conduction of the material. At the beginning of the transition process at $t = 0$, the volume charge drops exponentially

[2]The length of an XFEL bunch train is 600 μs containing up to 3000 bunches with a spacing of 200 ns. The default train repetition rate is 10 Hz. The number of X-rays per bunch is 10^{12} with energies between 3 and 15 keV.

as $\rho_{fr} = \rho_{fr}(0)$ exp $(-\gamma_1 t/\varepsilon_0)$. Consequently, the volume charge is reduced by a factor of $1/e$ within the relaxation time $t_0 = \varepsilon\varepsilon_0/\gamma_1$. The pulse duration of e.g. a Si detector of $\tau = R \cdot C_{st} \simeq 50$ ns can be achieved by a strip capacity $C_{st} = \varepsilon\varepsilon_0 S/d \simeq 1.5$ nF and an amplifier resistance $R \simeq 35$ Ohm, with $S \simeq 2.5 \cdot 10^{-5}$ m^2, the square of the strip surface and $d = 2$ μm, the layer spacing (pitch). The detector pulse duration should not be smaller than 30 % of the peaking time of the charge-sensitive amplifier, but should exceed approximately 10 ns and not be larger than the ILC bunch-to-bunch distance of about 300 ns.

Out of all abundant material silicon as sensitive material of the detector is proposed. The relaxation time of Si is however sizeably larger than the pulse duration time, but proper adjustment of the amplifier resistance can easily provide the required fast response of the detector before the next bunch arrives. The layout of the detector is schematically shown in Fig.11. Its sensitive region of 5 mm is composed of a series of 2500 individual Si layers, each 5x5 mm^2 in size and 2 μm thick[3]. The layers are separated by 0.05 μm SiO dielectric material. To read out the information, each layer is surrounded by a gold contact, 5 μm wide

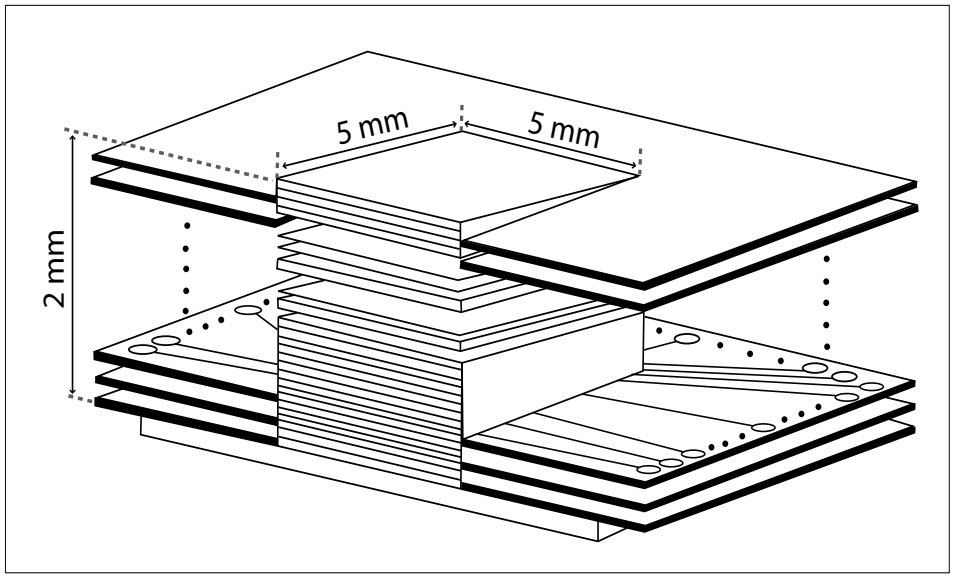

Figure 11: Silicon SR detector scheme with sub-μm spatial resolution.

and 0.9 μm thick, through which a charge-sensitive amplifier is connected. Charge collection in each layer is enabled by connecting the plus terminal of the external power supply. Some details of the detector structure and the readout scheme are shown in Fig.12. Readout electronics may be realized as simple and compact as used for e.g. the cathode strip readout of the muon chambers for the ATLAS experiment [16].

Such a detctor might be used for both schemes indicated in Fig.5. Since in the second scheme only soft photons with $E_\gamma < 20$ keV are selected the rate of γ-quanta emitted by 250 GeV electrons within 1 mm active Si material is $N_\gamma \simeq N_0(E_\gamma/E_{cr})^{1/3}/x_{SR} \simeq 3 \cdot 10^8$, where x_{SR} is the horizontal width of the SR fan of $\sim$80 mm. If we assume for each photoelectron an average energy loss of 3.6 eV per ionization process and a 30 % energy transfer from the photon to the photoelectrons, we expect on average 450 electrons per photon. Hence, about $1.4 \cdot 10^{11}$ electrons are eventually produced corresponding to a charge of $2.8 \cdot 10^8$ electrons in a 2 μm discrete detector layer. Accounting for a typical amplifier conversion factor of 5 mV/pC (Fig.12), an output signal with an amplitude of about 0.2 V is then expected. The measured charge in each layer

[3]Due to the expected smearing of the SR edges discussed in Sect.3 a detector with 2 μm pitch seems somewhat exaggerated. A pitch of 5 or 10 μm is probably more suitable for our purpose. In the GEANT simulations presented a pitch of 25 μm was assumed as an example. However, the final design of the radiation detector relies on several important not yet specified aspects such as the lay-out of the ILC BPM-based energy spectrometer, the space conditions downstream of the chicane and the background situation near the detector.

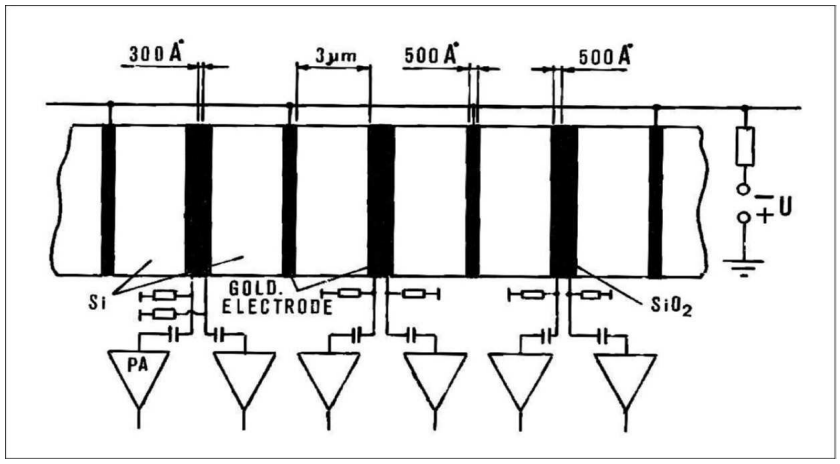

Figure 12: Detector structure and the scheme for the readout system.

provides, after amplification, precise information on the position of the photons since the energy of the γ-quanta is in good approximation homogeneously distributed in each layer.

For scheme 1, the number of photons entering the detector is orders of magnitude higher so that the signal expected is sufficiently large. Concerning radiation damage of the detector by indirect processes of generating electrons is thought to be less critical than for the Si strip detector. Although most of the low-energy photons are absorbed within the detector volume, most of them will not cause damages for the following reason. To remove an atom from the Si lattice an energy of at least 25 eV must be transfered. This requires a minimum energy for the electron of $\sim$270 keV, or about 300 keV for the incident photons. Thus, only a tiny fraction of the photons (see Fig.3) has the potential to cause detector damages. In addition, photons with energies larger than 1 MeV pass the 5 mm thick silicon detector with more than 90 % probability.

The technology for production of multilayer coatings is well developed in microelectronics industry. Methods for electron-beam sputtering and laser-induced evaporation are widely used in combination with precise layer thickness control by reflectometers.

6.3 Gas Amplification Detectors

As a second option for a μm-spatial resolution γ-ray detector we propose to employ a plane-parallel avalanche device with gas amplification in the range of 10 to 100. Schematically, the avalanche detector is a flat chamber with an anode-cathode gap of 1.5 mm filled with xenon at a pressure of 60 atm as indicated in Fig.13. The anode plane of the detector consists of 1 μm nickel (Ni) layers with 2 μm NiO dielectric separation from each other.

To eliminate edge effects, the sensitive detector elements are placed inside a plastic frame of 10x10 mm^2 covered by aluminum. The 10x10 mm^2 entrance window of the detector consists of a 1 mm thick berillium foil, which also acts as the high-voltage cathode plane. Since the path length of 20 keV photoelectrons in xenon at 1 atm is 20 mm [9], the distance between the anode and the cathode filled with Xe at 60 atm may be less than 1 mm resulting to a transverse avalanche size below 1 μm, the mean free path length of electrons under such conditions. Gas amplification of 10 to 100 corresponds to the first Townsend coefficient $\alpha_T \simeq$ 16-30 cm^{-1} for an anode-cathode distance of 1.5 mm. The coefficient α_T is given by the product $B \cdot E$ at high gas pressure, with E the electric field applied and B the xenon coefficient $3 \cdot 10^{-2}$ V^{-1}. Typical values of E are 0.5-0.8 kV/cm at an anode-cathode voltage of 150 V. Large numbers of photoelectrons are expected to be produced in the gas and a large fraction of them generates an output signal of about 100 mV for an amplifier conversion factor of 5 mV/pC.

Such avalanche detectors with characteristics needed for our purpose are widely used in heavy ion physics. Typical time resolutions achieved are in the range of 0.14 ns [17], and pulse-high amplitudes of 100 μA

(corresponding to a charge of 1 pC) were observed [18]. These detectors are also quite resistant to radiation damages. They can for example withstand radiation doses of $2 \cdot 10^9 cm^{-2} s^{-1}$ [19].

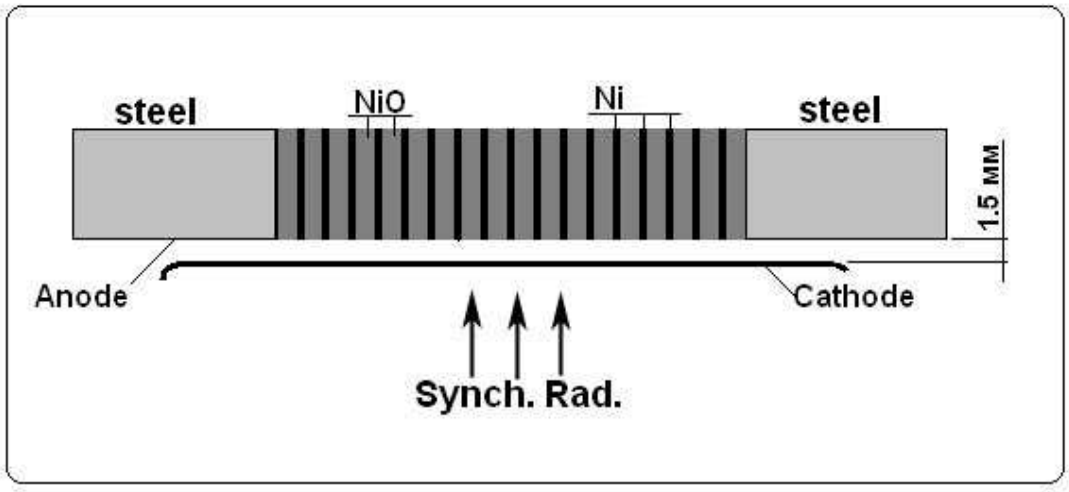

Figure 13: Scheme of gas amplification detector with sub-μm spatial resolution.

7 Conclusions

The proposed method for a bunch-to-bunch beam energy measurements at the ILC relies on monitoring synchrotron radiation light emitted from electrons and positrons passing the magnets of an energy spectrometer. Measuring the width respectively the endpoints of the horizontal SR fan sufficiently downstream of the spectrometer permits to determine the beam energy with an accuracy better than 10^{-4}. Advantages of such an approach consist on its simple scheme and of being largely insensitive to jitters of the beam position, the beam angle and vibrations of the set-up elements.

Two basic schemes for monitoring E_b are proposed. The first one relies on measuring the width of the direct SR fan by means of high-spatial resolution photon detectors located downstream of the spectrometer. Since the sensors are positioned in an intense synchrotron radiation enviroment serious problems due to radiation damage are expected and precautions are necessary. Large irradiation of the detectors can be avoided if soft photons are extracted by mirrors located in the beamline. This option, denoted as scheme 2, leads to large γ-ray displacements and the detectors can be placed out of the intense SR yield so that important damage-producing interactions are to a great extent avoided.

Concerning possible detector schemes, standard silicon strip detectors often applied in particle physics experiments are suggested for measuring the width of the SR fan with the necessary micrometer precision. If however such detectors would be positioned into the high-intense synchrotron radiation enviroment serious damages are expected. Therefore, it is proposed to employ silicon strip sensors only if scheme 2 will be realized. In addition, novel high-spatial resolution detectors are proposed to perform precise SR fan edge determinations. One of the detector options discussed consists of about 2500 independen 2 μm Si layers, each separated by 0.05 μm SiO dielectric. Appropriate readout electronics can be made simple and compact. As a second option for a high-spatial resolution detector a plane-parallel avalanche detector might be employed. A basic layout of such a device is discussed and parameters as needed for our purpose have been achieved in heavy-ion physics applications. However, for both detector options R&D is needed, but realization of such devices seems possible by means of methods developed by microelectronic industry.

Preliminary GEANT simulations with realistic assumptions support prospects to achieve a sensitivity of 10

μm/25 MeV. Scaling this sensitivity to a detector with spatial resolution of 2 μm permits to reach an energy uncertainty of $\Delta E_b/E_b$ better than 10^{-4} for the nominal 250 GeV ILC beam energy.

The $1/E_b$ energy dependence of the sensitivity of the method implies a reduced precision at higher beam energies, while at the Z pole with $E_b \simeq 46$ GeV the sensitivity is enhanced. This is in accord with the somewhat stronger demands for $\Delta E_b/E_b$ as discussed e.g. in [20] which might be difficult to achieve for a BPM-based energy spectrometer.

We would like to emphasize that if besides the beam position monitor-based spectrometer method as the standard tool for beam energy measuremnts upstream of the interaction point a complementary technique will be employed redundancy and reliability of the results is provided.

Acknowledgments

We would like to thank Andriy Ushakov for valuable discussions and energy deposite calculation by means of the FLUKA code.

References

[1] V.N. Duginov et al., The Beam Energy Spectrometer at the International Linear Collider, LC-DET-2004-031.

[2] I. Meshkov, T. Mamedov and E. Syresin, An electron/positron energy monitor based on synchrotron radiation, contribution to the Beam Energy Meeting, Dubna, May 2003.

[3] K. Hiller, Beam Energy Measurement by Synchrotron Radiation, contribution to the Beam Energy Meeting, Yerevan, May 2005.

[4] J. Kent et al., SLAC-PUB-5110 (1990).

[5] S. Herztbach, Proceedings of the LCWS 200, Batavia, Illinois, October 2000.

[6] GEANT, Detector Description and Simulation Tool, CERN Program Linrary Long Write-up W5013 (1994).

[7] D.K.G. De Boer and W.W. van den Hoogenhof, Adv. X-ray Anal. 34 (1991) 35.

[8] N. Muchnoi et al., paper submitted to EPAC, Edinburgh UK, 26-30 June 2006; R. Klein et al., Nucl. Inst. Meth. A 384 (1997) 293.

[9] G. Charpak, Nucl. Inst. Meth. 156 (1978) 1.

[10] A.P. Babichev et al., Physical values, Energoatomisdat (1991).

[11] F.-W. Sadrozinski, IEEE Trans. on Nucl. Sci. 45 (1998) 295.

[12] G.Lutz, Jour. of Synch. Rad. 13 (2006) 99.

[13] V.A.J. van Lint, Nucl. Instrum. Meth. A253 (1987) 453; H.W. Kramer, Nucl. Inst. Meth. in Phys. Res. A225 (1984) 615; IEEE Trans. Nucl. Sci. NS, 29, No.3 (1982) 1088.

[14] The Technical Design Report of the European XFEL, July 2006, *http://xfel.desy.de/tdr/index_eng.html*.

[15] L.A. Bessonov, Theoretical base of electrotechnique, Vyshshaj shkola, 1986.

[16] ATLAS Muon Spectrometer, Technical Design Report, June, 1997.

[17] A. Bereskin and N. Zwang, Nucl. Inst. Meth. 144 (1977) 609.

[18] Y. Eyal and H. Stelzer, Nucl. Inst. Meth. 155 (1978) 157.

[19] G. Gaukler et al., Nucl. Inst. Meth. 141 (1977) 115.

[20] P.C. Rowson and M. Woods, SLAC-PUB 8745, hep-ex/0012055;
R. Hawkings and K. Moenig, DESY 99-157, 1999.